

Gapped Excitations in the High-Pressure Antiferromagnetic Phase of URu₂Si₂

T.J. Williams,^{1,2,*} H. Barath,³ Z. Yamani,⁴ J.A. Rodriguez-Riviera,^{5,6} J.B. Leão,⁵
J.D. Garrett,⁷ G.M. Luke,^{1,7,8} W.J.L. Buyers,^{4,8} and C. Broholm^{3,5,†}

¹*Department of Physics and Astronomy, McMaster University, Hamilton, ON, Canada, L8S 4M1*

²*Quantum Condensed Matter Division, Neutron Sciences Directorate,
Oak Ridge National Lab, Oak Ridge, TN, 37831, USA*

³*Institute for Quantum Matter and Department of Physics and Astronomy,
Johns Hopkins University, Baltimore, MD, USA, 21218*

⁴*National Research Council, Chalk River Laboratories, Chalk River, ON, Canada, K0J 1J0*

⁵*NIST Center for Neutron Research, National Institute of Standards and Technology, Gaithersburg, MD, USA, 20899*

⁶*Department of Materials Science and Engineering,
University of Maryland, College Park, MD, USA, 20740*

⁷*Brockhouse Institute for Materials Science, McMaster University, Hamilton, ON, Canada, L8S 4M1*

⁸*Canadian Institute for Advanced Research, Toronto, Ontario, Canada, M5G 1Z8*

(Dated: February 10, 2022)

We report a neutron scattering study of the magnetic excitation spectrum in each of the three temperature and pressure driven phases of URu₂Si₂. We find qualitatively similar excitations throughout the (*HOL*) scattering plane in the hidden order and large moment phases, with no changes in the $\hbar\omega$ -widths of the excitations at the $\Sigma = (1.407, 0, 0)$ and $Z = (1, 0, 0)$ points, within our experimental resolution. There is, however, an increase in the gap at the Σ point and an increase in the first moment of both excitations. At 8 meV where the \mathbf{Q} -dependence of magnetic scattering in the hidden order phase is extended in \mathbf{Q} -space, the excitations in the large moment phase are sharper. The expanded \mathbf{Q} - $\hbar\omega$ coverage of this study suggest more complete nesting within the antiferromagnetic phase, an important property for future theoretical predictions of a hidden order parameter.

PACS numbers: 78.70.Nx, 71.27.+a

The heavy fermion material URu₂Si₂ exhibits a specific heat anomaly at $T_0 = 17.5$ K indicative of a second order phase transition [1, 2]. Decades of research notwithstanding [3–6], an order parameter characterizing the putative symmetry breaking of the low temperature phase has not been identified. Neutron scattering does show antiferromagnetic order with an ordering wavevector $\mathbf{Q}_m = (1, 0, 0)$, but the small sample-averaged moment of $0.03 \mu_B$ [2], seems hard to reconcile with a change in entropy $\Delta S = 0.24R \ln 2$ [1] through the transition. This moment may be intrinsic [7] or may arise from heterogeneous inclusions of a large moment phase [8]. Spin fluctuations with a characteristic wave vector $(1 \pm \delta, 0, 0)$ ($\delta = 0.407(6)$) are observed in the paramagnetic (PM) phase, indicative of Fermi-surface nesting at the Σ point, which for URu₂Si₂ occurs for $\delta = \frac{1}{2}(1 - (a/c)^2) = 0.406$ ($a=4.128$ Å and $c=9.534$ Å at $T=4$ K) [9]. Below T_0 , in the so-called ‘hidden order’ (HO) phase, these excitations become gapped as for a spin density wave transition and concordant with the specific heat anomaly, but without development of the attendant staggered magnetization.

Hydrostatic pressure of ~ 0.6 GPa replaces the HO phase with a large-moment antiferromagnetic (AF) phase with an ordered magnetic moment of $0.3 \mu_B$ [10, 11]. Here we show the gapped excitations at the $\Sigma = (1.407, 0, 0)$ and $Z = (1, 0, 0)$ points persist in the

AF phase, albeit with an enhanced gap at the Σ point in the high pressure phase. Our results are not inconsistent with previous experimental data [10, 12, 13], though our results clearly show the existence of an inelastic signal at the Z point. However, in this work, the expanded coverage of \mathbf{Q} - E space reveals a similarity between magnetic excitations in the two low temperature phases that was not previously appreciated.

High quality single crystals of URu₂Si₂ were grown by the Czochralski method in a tri-arc furnace. Three crystals with a total mass of approximately 37 g were coaligned in the (*HOL*) plane for the ambient pressure measurements. A single crystal with a mass of 1.66 g was cut by spark erosion and aligned in the (*HOL*) plane and placed inside a 13-8Mo steel He-gas pressure vessel and was connected to a commercially available pressurizing intensifier through a heated high-pressure capillary. Pressure was adjusted only at temperatures well above the helium melting curve and the capillary was heated during slow cooling of the cell to accommodate the contracting He gas, thus minimizing pressure loss and pressure inhomogeneities across the sample space. The pressure cell was allowed to cool under constant pressure to the freezing point of helium. Pressure calibrations were previously done using the lattice constants change in highly oriented pyrolytic graphite crystals. The neutron scattering measurements were performed on the Multi-Axis Crystal Spectrometer (MACS) at the NIST Center for Neutron Research, where a 20 MW reactor, a dedicated liquid H₂ moderator, and a doubly-focusing PG(002) monochromator provides an incident

*Electronic address: williamstj@ornl.gov

†Electronic address: broholm@jhu.edu

beam flux of 2.0×10^8 n/cm²/s [14] for an initial energy $E_i = 3.6$ meV. In the vicinity of (1,0,0), the in-plane resolution was 0.12 \AA^{-1} along L , 0.043 \AA^{-1} along H , and the out-of-plane resolution was 0.24 \AA^{-1} at zero energy transfer. All measurements were performed using a fixed $E_f = 5.054$ meV, with an energy resolution of 0.45 meV. Twenty detection channels permitted efficient mapping of inelastic scattering throughout the $(H0L)$ plane. Measurements were performed at ambient pressure and $T = 25$ K in the paramagnetic phase, at ambient pressure and $T = 2$ K in the hidden order phase, and at a pressure of $P = 1.02$ GPa and $T = 4$ K in the AF phase.

Phonon scattering near (0,0,2) is visible in both the paramagnetic (Fig. 1(a)) and hidden order (Fig. 1(b)) phases. This allowed for normalization of the data so that we can provide absolute values of the scattering cross sections in each phase, which are consistent with previously published values [15]. To isolate scattering from URu₂Si₂ from that associated with the massive pressure cell and the helium pressure medium, a background was measured for the pressure cell with the sample exchanged by an equal volume of aluminum pressurized to 1.02 GPa. The scattering intensity under pressure was also subject to normalization using the (0,0,2) structural Bragg peak, which showed the transmission of the pressure cell is 18%, consistent with direct measurements. We attribute all of the scattering at (1,0,0) to magnetic scattering and the normalization yields a cross section for the (1,0,0) magnetic Bragg peak of $0.36(9) \mu_B$, in good agreement with the previously reported ordered moment in the AF phase [10]. In addition, all data was corrected for the effects of higher order contamination on the monitor count rate [14].

The inelastic scattering cross section along high symmetry directions in the $(H0L)$ plane for the three different phases is shown in Fig. 1. The upper and middle panels show the momentum and energy transfer dependence of the magnetic scattering in the PM and HO phases, respectively, which are consistent with earlier findings [2, 9, 16]. There are substantial changes across the PM to HO phase transition. In the PM phase, the scattering takes the form of gapless ridges with most of the intensity at the Σ point though a ridge is also clearly discerned at the Z point. In the HO phase, well-defined gaps have opened at both the Z and Σ points, and the intensity at the Z point has increased. The lowest panel shows data in the AF phase. Due to the pressure cell the quality of these data is significantly reduced. The overall $\mathbf{Q} - \hbar\omega$ dependent scattering is qualitatively similar to that of the HO phase, though the gap at the Σ point is considerably enhanced.

Further comparisons between the three phases can be made by examining the constant energy transfer slices through the $(H0L)$ zone data, shown in Fig. 2. The figure shows the average intensity in 1 meV-thick slices centered at 2 meV, 5 meV, 8 meV and 11 meV. For improved statistics, we have symmetrized the data and present a

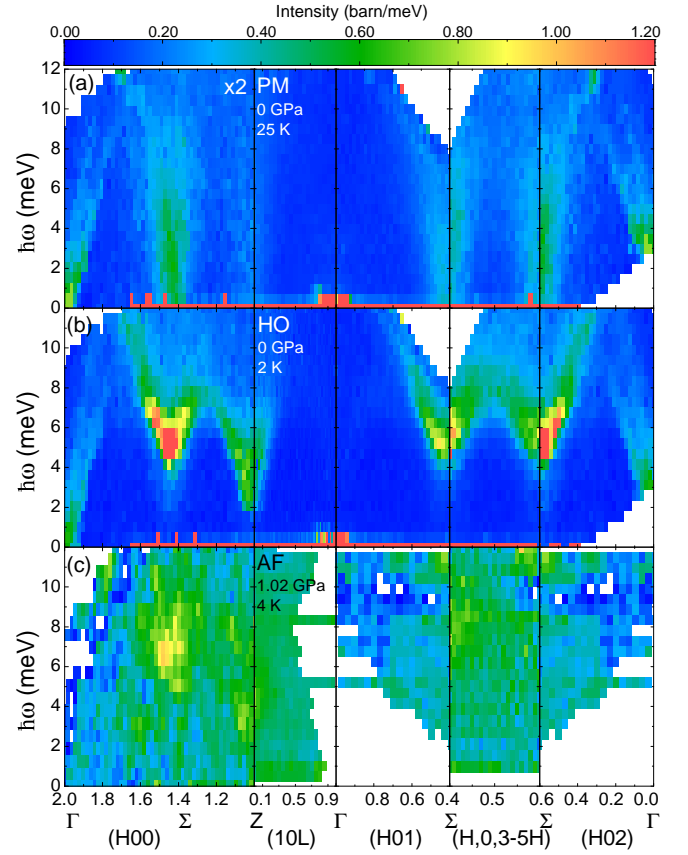


FIG. 1: (Color online) The scattering intensity as a function of energy and scattering vector along various high symmetry directions in the $(H0L)$ plane in the three phases studied: (a) at ambient pressure and 25K, in the paramagnetic (PM) phase. The data has been scaled up by a factor of 2 to make the scattering more visible. The phonon at (2,0,0) is visible, as are the excitations at the Σ point. (b) at ambient pressure and 2 K, in the HO regime. The phonon is present with equal intensity, while the excitations at (1.4,0,0) have become gapped, and more weakly dispersing. The excitation at the Z point is also present. (c) at 1.02 GPa and 4 K, in the AF phase. The scattering here looks qualitatively similar to the spectrum in the HO phase, albeit with a larger gap at the Σ point, but not at the Z point.

single quadrant at each energy transfer. While the excitations at the Σ point are present in all three phases, intensity at the Z point is mainly visible in the HO and AF phases. In the HO phase, there is considerably more spectral weight in all of the excitations compared to the PM phase. Comparing the HO and AF phase, we see in the 5 meV slice that the gap in the AF phase is larger at the Σ points. Both modes are observed in the HO phase at 5 meV, while only the excitations at the Z point are seen in the corresponding AF slice. The Z and Σ modes have similar intensity at 8 meV within the AF phase compared to 5 meV in the HO phase. In the HO phase, the 8 meV data consists of smooth ridges, while well-defined points in reciprocal space are still visible at 8 meV in the

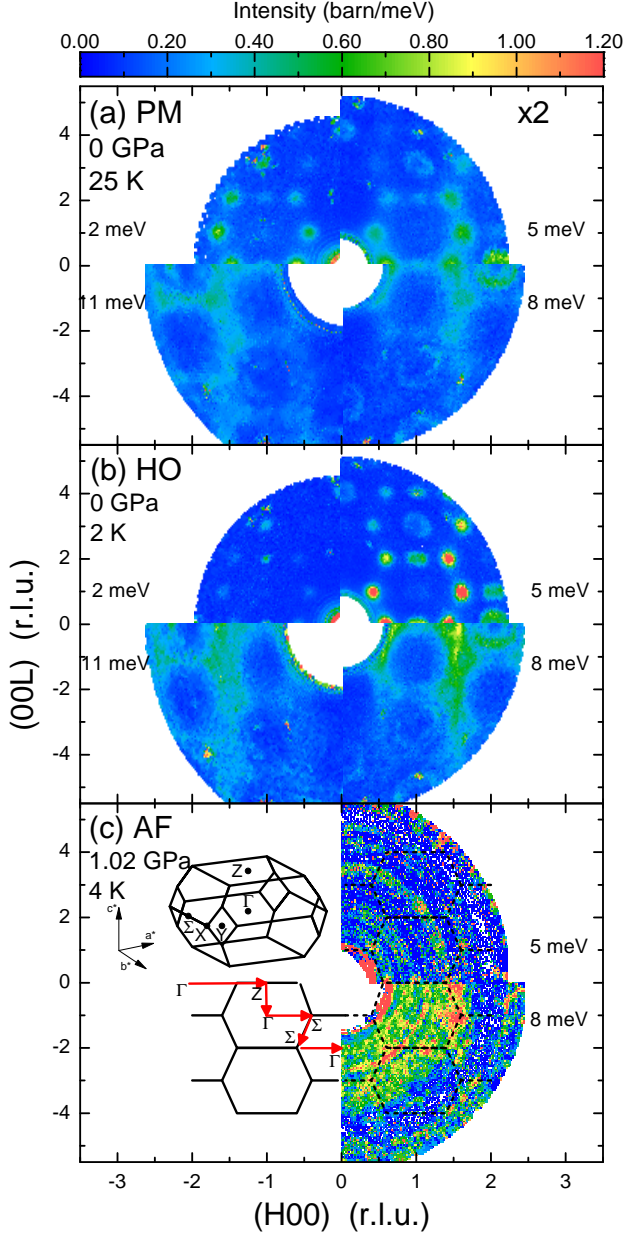


FIG. 2: (Color online) Constant energy slices in the $(H0L)$ plane in each of the three phases. Energies shown are 2 meV, 5 meV, 8 meV and 11 meV (clockwise from top left). The range of integration of energies for the slices was ± 0.5 meV and the bin size is 0.013 \AA^{-2} . The data in the PM phase (panel (a)) has been scaled up by a factor of 2, as in Fig. 1. The lower left of the figure shows the Brillouin zone of URu_2Si_2 , with the arrows indicating the directions measured in Fig. 1.

AF data.

For a quantitative spectral analysis, the energy dependence of the scattering at Z and Σ in the three phases are shown in Fig. 3. These cuts were extracted from the

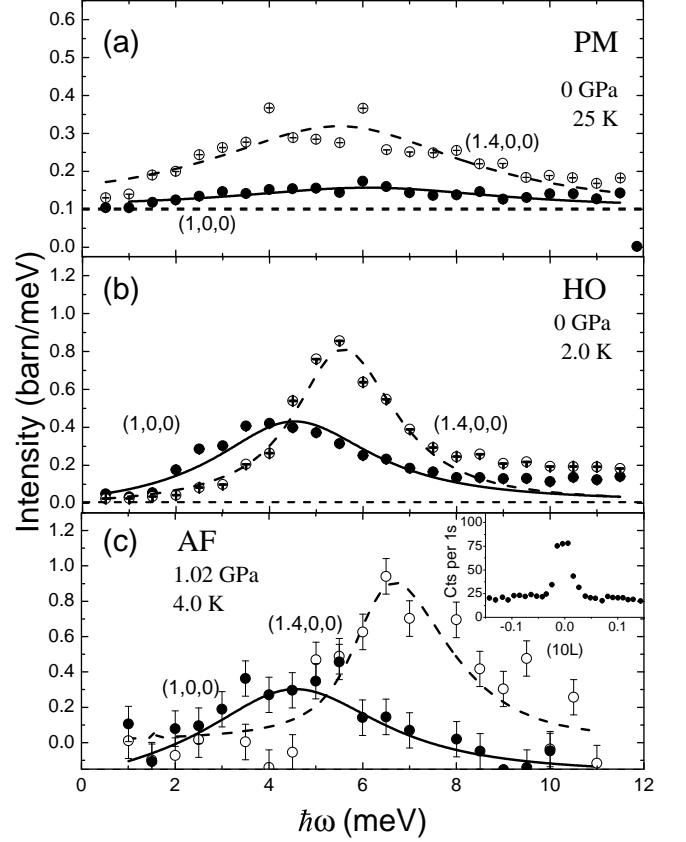


FIG. 3: (Color online) The energy-dependence of the scattering intensity for crystal momentum Z (filled circles) and Σ (open circles) in each phase. The error bars represent $\pm 1\sigma$, while the lines are fits as described in the text, with the horizontal lines showing the fitted background. (a) In the PM phase, a weak and broad spectrum of scattering is seen at Z , with a more pronounced but also broad peak at Σ . (b) In the HO phase, the scattering is much more intense at both wave vectors and intensity at Σ has shifted to higher energy. (c) In the AF phase, both peaks are still present; the peak at $(1.4,0,0)$ seems to have shifted to slightly higher energies. Note: the fitted background lies below the axis here, due to the subtraction described in the text. (inset) The scattering along $(10L)$ in the AF phase shows the substantially more intense peak at $(1,0,0)$, arising from the large AF moment.

same data that is shown in Fig. 1 and Fig. 2. Following the analysis of [17], the data in each phase was fit to the resolution-convoluted line shape associated with the following expression for the low temperature magnetic scattering cross section near the Z and Σ points:

$$\tilde{I}(\mathbf{Q}, \omega) = \frac{\mathcal{A}}{\epsilon(\mathbf{Q})} \cdot \frac{1 - e^{-\beta\Delta}}{1 - e^{-\beta\hbar\omega}} \cdot \left[\frac{\hbar\gamma/\pi}{(\hbar\omega - \epsilon(\mathbf{Q}))^2 + (\hbar\gamma)^2} - \frac{\hbar\gamma/\pi}{(\hbar\omega + \epsilon(\mathbf{Q}))^2 + (\hbar\gamma)^2} \right] \quad (1)$$

where $\hbar\gamma$ is the spectral Half Width at Half Maximum (HWHM) and $\mathcal{A} \approx \hbar^2 \int \tilde{I}(\mathbf{Q}, \omega) \omega d\omega$ approximates the first moment in the limit where $\hbar\gamma \ll \epsilon(\mathbf{Q})$. With an

energy gap Δ , the phenomenological dispersion relation reads:

$$\epsilon(\mathbf{Q}) = \sqrt{\Delta^2 + \hbar^2(\delta Q_\perp^2 v_\perp^2 + \delta Q_\parallel^2 v_\parallel^2)} \quad (2)$$

Here $\delta Q_{\perp,\parallel} = |(\mathbf{Q} - \mathbf{Q}_0)_{\perp,\parallel}|$ is the projection of the deviation wave vector transfer \mathbf{Q} from the critical wave vector \mathbf{Q}_0 perpendicular and parallel, respectively, to the $\hat{\mathbf{c}}$ -direction. We take the velocity to be isotropic within the tetragonal basal plane because the present data from the ($H0L$) zone only is insensitive to potential in-plane anisotropy allowed by symmetry in the low T phases. The velocities used were determined from the HO phase, using the data in Fig. 1(b), and were found to be $v_H = v_K = v_\perp = 23.7(5)$ meV·Å and $v_L = v_\parallel = 32.5(7)$ meV·Å. Eq. 1 was convoluted with the 4D instrumental resolution function using RESLIB [18]. In order to extract reliable measurements of the energy gaps at both \mathbf{Q} -points, this fitting was performed for a variety of integration ranges in both H and L . The values of the gap, Δ , and width, $\hbar\gamma$, versus the integration area (in Å⁻²) were then extrapolated to the size of the resolution ellipse given by RESLIB. This allowed these parameters to be determined in a way that was only dependent on the instrumental resolution and not the integration range chosen to form the energy scan from the \mathbf{Q} -dependent data. The results of this fitting are summarized in Table I. The error bars given for the values of Δ and $\hbar\gamma$ are a combination of the errors resulting from the RESLIB fits as well as the extrapolation described above.

Phase	Wavevector	\mathcal{A} (barn · meV)	Δ (meV)	$\hbar\gamma$ (meV)
PM	Z	1.00(8)	2.3(5)	2.4(4)
PM	Σ	3.0(2)	2.2(6)	1.8(2)
HO	Z	4.3(3)	2.3(4)	0.9(1)
HO	Σ	5.1(3)	4.2(2)	0.7(1)
AF	Z	5.8(6)	2.3(4)	0.9(2)
AF	Σ	6.1(1.5)	5.5(3)	0.7(1)

TABLE I: Results of fitting the data in Fig. 3 to the dispersion in Eq. 1. The determination of the errors for Δ and $\hbar\gamma$ are described in the text, while the error bars given for \mathcal{A} are a combination of the fitting error and the error from the normalization, which was 6.3%. The errors resulting from the transmission of the pressure cell difficult to estimate and so are not included in the error of \mathcal{A} , though these effects should not affect the values or errors of Δ and $\hbar\gamma$.

In the HO phase, the excitation at the Σ point becomes gapped, with $\Delta = 4.2(2)$ meV. Upon entering the AF phase this gap increases to $\Delta = 5.5(3)$ meV, while the physical half width extracted from this analysis is $\hbar\gamma = 0.7(1)$ meV, identical in these two phases. At the Z point the spectrum is indistinguishable in the two phases. Note that the values for the gap and half width $\Delta = 2.3(4)$ meV and $\hbar\gamma = 0.9(2)$ meV are both larger than literature values [7] and this may be a result of the coarser \mathbf{Q} -resolution of the present measurement.

The main difference in the scattering in the AF phase as compared to the HO phase is the increased value of the first moment, \mathcal{A} , and the additional Bragg scattering at (1,0,0). Both of these results point to strengthening of antiferromagnetic order. The inset to Fig. 3(c) shows a transverse cut through the (1,0,0) elastic peak, the intensity of which corresponds to a moment size of $0.36(9) \mu_B$. This is evidence that the measurements were indeed conducted in the AF phase. Our observation of inelastic scattering at Z is not a surprise given the enhanced AF order. In previous, lower pressure work an inelastic peak was observed at Z for $P = 0.72$ GPa [10] but not for $P = 0.62$ GPa [13]. A possible explanation for all three neutron experiments under pressure is that the Z mode softens at the critical pressure and so falls within the elastic line in the lower pressure measurements. This would be consistent with recent high pressure Raman data [19].

We also note that the \mathbf{Q} -widths of the excitations in Fig. 1 in the AF phase are similar to those of the HO phase, where it has broadened in \mathbf{Q} as compared to the PM excitations. This suggests that the velocities of the excitations are very similar in the HO and AF phases. This is also readily visible in Fig. 1, where we observe the merger of the dispersing modes around 8 meV in both the AF and HO phases. This extends previous work in the AF, where only the $\hbar\omega$ -width was measured. Between the paramagnetic and hidden order phases, there is significant Fermi surface reconstruction, based on transport and thermodynamic measurements [1, 20]. Somewhat surprisingly, there are no dramatic changes in the Fermi surface properties upon entering the AF phase, as seen by resistivity [21], and quantum oscillation measurements [22]. Together with the qualitative similarities of the spin correlations seen in this experiment, this suggests that there is very little change in the electronic properties between the hidden order phase and the antiferromagnetic phase.

Within a nesting picture, these results suggest more complete nesting with a larger first moment in the AF phase. The applied pressure shifts the resonance to slightly higher energies, but only at the Σ point. The increase in the first moment of both the Σ and Z point excitations, as well as the increase in the size of the ordered moment in the AF phase suggests that there must be a loss of intensity at higher energies. This would indicate that the AF state is more coherent with a more localized magnetic moment. Furthermore, the enhancement of the first moment in the AF state would imply a reduction in energy scale the magnetic exchange due to the first moment sum rule [23].

Previous work attributes the presence of gapped excitations at the Σ and Z points as signatures of the HO phase [24]. The present data shows that entering the AF phase does not weaken or destroy either set of excitations, but rather increases the intensity of both and increases the gap at the Σ point. In fact, the application of the hydrostatic pressure that gives rise to the AF phase does not suppress the HO transition, but actually

increases T_0 , before the AF phase emerges [25]. The measurements presented here form a complete spectroscopic study of the paramagnetic, ‘hidden order’ and antiferromagnetic phases of URu_2Si_2 . The enhancement of the first moment, \mathcal{A} , in the AF state, combined with no observed changes in the \mathbf{Q} -width or energy width ($\hbar\gamma$) of the excitations, will form an important set of constraints for theoretical models of the HO phase, which can now be more directly compared to the AF phase under pressure.

Acknowledgments

The authors would like to thank M.B. Stone for help with the data analysis. Work at IQM was supported by

DoE, Office of Basic Energy Sciences, Division of Materials Sciences and Engineering under award DE-FG02-08ER46544. This work utilized facilities supported in part by the National Science Foundation under Agreement No. DMR-1508249. Research at McMaster University is supported by NSERC. T.J.W. acknowledges support from the Wigner Fellowship program at Oak Ridge National Laboratory.

-
- [1] T.T.M. Palstra, A.A. Menovsky, J. van den Berg, A.J. Dirkmaat, P.H. Kes, G.J. Nieuwenhuys and J.A. Mydosh. *Phys. Rev. Lett.* **55**, 2727 (1985).
 - [2] C. Broholm, J.K. Kjems, W.J.L. Buyers, P. Matthews, T.T.M. Palstra, A.A. Menovsky and J.A. Mydosh. *Phys. Rev. Lett.* **58**, 1467 (1987).
 - [3] D.A. Bonn, J.D. Garrett and T. Timusk. *Phys. Rev. Lett.* **61**, 1305 (1988).
 - [4] W.J.L. Buyers, Z. Tun, T. Peterson, T.E. Mason, J.-G. Lussier, B.D. Gaulin and A.A. Menovsky. *Physica B* **199&200**, 95 (1994).
 - [5] T.E. Mason, W.J.L. Buyers, T. Peterson, A.A. Menovsky and J.D. Garrett. *J. Phys.: Condens. Matter* **7**, 5089 (1995).
 - [6] F. Bourdarot, A. Bombardi, P. Burlet, M. Enderle, J. Flouquet, P. Lejay, N.Kernavainois, V.P. Mineev, L.Paolasini, M.E. Zhitomirsky and B. Fåk. *Physica B* **359-361**, 986 (2005).
 - [7] F. Bourdarot, S. Raymond and L.-P. Regnault. *Phil. Mag.* **94**, 3702 (2014).
 - [8] S. Takagi, S. Ishihara, S. Saitoh, H.-i. Sasaki, H. Tanida, M. Yokoyama and H. Amitsuka. *J. Phys. Soc. Japan*. **76**, 033708 (2007).
 - [9] C.R. Wiebe, J.A. Janik, G.J. MacDougall, G.M. Luke, J.D. Garrett, H.D. Zhou, Y.-J. Jo, L. Balicas, Y. Qiu, J.R.D. Copley, Z. Yamani and W.J.L. Buyers. *Nature Physics* **3**, 96 (2007).
 - [10] D. Aoki, F. Bourdarot, E. Hassinger, G. Knebel, A. Miyake, S. Raymond, V. Taufour and J. Flouquet. *J. Phys. Soc. Jap.* **78**, 053701 (2009).
 - [11] N.P. Butch, J.R. Jeffries, S. Chi, J.B. Leão, J.W. Lynn and M.B. Maple. *Phys. Rev. B*. **82**, 060408(R) (2010).
 - [12] E. Hassinger, D. Aoki, F. Bourdarot, G. Knebel, V. Taufour, S. Raymond, A. Villaume and J. Flouquet. *J. Phys.: Conf. Ser.* **251**, 012001 (2010).
 - [13] F. Bourdarot, E. Hassinger, S. Raymond, D. Aoki, V. Taufour, L.-P. Regnault and J. Flouquet. *J. Phys. Soc. Jap* **78**, 064719 (2010).
 - [14] J.A. Rodriguez, D.M. Adler, P.C. Brand, C. Broholm, J.C. Cook, C. Brocker, R. Hammond, Z. Huang, P. Hundertmark, J.W. Lynn, N.C. Maliszewskyj, J. Moyer, J. Orndorff, D. Pierce, T.D. Pike, G. Scharfstein, S.A. Smee and R. Vilaseca. *Meas. Sci. Technol.* **19**, 034023 (2008).
 - [15] N.P. Butch, M.E. Manley, J.R. Jeffries, M. Janoschek, K. Huang, M.B. Maple, A.H. Said, B.M. Leu and J.W. Lynn. *Phys. Rev. B*. **91**, 035128 (2015).
 - [16] C.R. Wiebe, G.M. Luke, Z. Yamani, A.A. Menovsky and W.J.L. Buyers. *Phys. Rev. B* **69**, 132418 (2004).
 - [17] C. Broholm, H. Lin, P.T. Matthews, T.E. Mason, W.J.L. Buyers, M.F. Collins, A.A. Menovsky, J.A. Mydosh and J.K. Kjems. *Phys. Rev. B* **43**, 12809 (1991).
 - [18] A. Zheludev: *ResLib 3.4* (Oak Ridge National Laboratory, (2007).
 - [19] G. Blumberg. Private communication.
 - [20] M.B. Maple, J.W. Chen, Y. Dalichaouch, T. Kohara, C. Rossel, M.S. Torikachvili, M.W. McElfresh and J.D. Thompson. *Phys. Rev. Lett.* **56**, 185 (1986).
 - [21] M.W. McElfresh, J.D. Thompson, J.O. Willis, M.B. Maple, T. Kohara and M.S. Torikachvili. *Phys. Rev. B* **35**, 43 (1987).
 - [22] E. Hassinger, G. Knebel, T.D. Matsuda, D. Aoki, V. Taufour and J. Flouquet. *Phys. Rev. Lett.* **105**, 216409 (2010).
 - [23] J. Leiner, V. Thampy, A.D. Christianson, D.L. Abernathy, M.B. Stone, M.D. Lumsden, A.S. Sefat, B.C. Sales, J. Hu, Z. Mao, W. Bao and C. Broholm. *Phys. Rev. B*. **90**, 100501(R) (2014).
 - [24] A. Villaume, F. Bourdarot, E. Hassinger, S. Raymond, V. Taufour, D. Aoki and J. Flouquet. *Phys. Rev. B* **78**, 012504 (2008).
 - [25] G. Motoyama, T. Nishioka and N.K. Sato. *Phys. Rev. Lett.* **90**, 166402 (2003).